

# Circular polarization of gravitational waves from non-rotating supernova cores: a new probe into the pre-explosion hydrodynamics

Kazuhiro Hayama<sup>1</sup>, Takami Kuroda<sup>2</sup>, Kei Kotake<sup>3</sup>, and Tomoya Takiwaki<sup>4</sup>

<sup>1</sup> *KAGRA Observatory, Institute for Cosmic Ray Research, University of Tokyo, 238 Higashi Mozumi, Kamioka, Gifu 506-1205, Japan*

<sup>2</sup> *Institut für Kernphysik, Technische Universität Darmstadt Schlossgartenstrasse 9, D-64289 Darmstadt, Germany*

<sup>3</sup> *Department of Applied Physics, Fukuoka University, Jonan, Nanakuma, Fukuoka 814-0180, Japan*

<sup>4</sup> *Division of Theoretical Astronomy, National Astronomical Observatory of Japan (NAOJ), 2-21-1, Osawa, Mitaka, Tokyo, 181-8588, Japan*

26 July 2021

## ABSTRACT

We present an analysis of the circular polarization of gravitational-waves (GWs) using results from three-dimensional (3D), general relativistic (GR) core-collapse simulations of a non-rotating  $15M_{\odot}$  star. For the signal detection, we perform a coherent network analysis taking into account the four interferometers of LIGO Hanford, LIGO Livingston, VIRGO, and KAGRA. We focus on the Stokes  $V$  parameter, which directly characterizes the asymmetry of the GW circular polarization. We find that the amplitude of the GW polarization becomes bigger for our 3D-GR model that exhibits strong activity of the standing accretion shock instability (SASI). Our results suggest that the SASI-induced accretion flows to the proto-neutron star (PNS) lead to a characteristic, low-frequency modulation (100  $\sim$  200 Hz) in both the waveform and the GW circular polarization. During the vigorous SASI phase, we observe that the GW polarization switches from the right- to left-handed mode, which is clearly visible in the spectrogram. By estimating the signal-to-noise ratio of the GW polarization, we demonstrate that the detection horizon of the circular polarization extends by more than a factor of several times farther comparing to that of the GW amplitude. Our results suggest that the GW circular polarization, if detected, could provide a new probe into the pre-explosion hydrodynamics such as the SASI activity and the  $g$ -mode oscillation of the PNS.

**Key words:** stars: interiors – stars: massive – supernovae: general.

## 1 INTRODUCTION

The LIGO and Virgo collaboration has made the first joint detection of gravitational waves (GWs) from merging binary system of black holes (Abbott et al. 2017, 2016). The network of the *three* detectors has not only enabled to improve the sky localization of the source significantly, but also probe the GW polarization for the first time (Abbott et al. 2017), the latter of which was difficult for the twin LIGO detectors having similar orientations. With KAGRA (Akutsu et al. 2017), the four-detector era is coming soon. The network of these advanced GW detectors is expected to unravel the yet-uncertain nature of astrophysical sources (e.g., Sathyaprakash & Schutz (2009)), which include core-collapse supernovae (CCSNe, e.g., Janka (2017) for a review).

Extensive numerical simulations have been done so far to study the GW signatures from CCSNe in different contexts (e.g., Cerdá-Durán et al. (2013); Ott et al. (2013); Yakunin et al. (2015); Kuroda et al. (2014); Morozova et al.

(2018) and Kotake (2013); Ott (2009) for a review). For canonical supernova progenitors (Heger et al. 2005), core rotation is generally too slow to affect the dynamics (e.g., Takiwaki et al. (2016); Summa et al. (2017)). For such progenitors, the GW signatures in the postbounce phase are characterized by prompt convection, neutrino-driven convection, proto-neutron star (PNS) convection, the standing accretion shock instability (SASI), and the  $g$ (/f)-mode oscillation of the PNS surface (e.g., Müller & Janka (1997); Müller et al. (2004); Murphy et al. (2009); Kotake et al. (2009); Müller et al. (2013); Morozova et al. (2018)). Among them, the most distinct GW emission process generically seen in recent self-consistent three-dimensional (3D) models is the one from the PNS oscillation (Kuroda et al. 2016; Andresen et al. 2017; Yakunin et al. 2017). The characteristic GW frequency increases almost monotonically with time due to an accumulating accretion to the PNS, which ranges approximately from  $f_{\text{PNS}} \sim 100$  to 1000 Hz. On the other hand, the typical

frequency of the SASI-induced GW signals is concentrated in the lower frequency range of  $f_{\text{SASI}} \sim 100$  to 250 Hz and persists when the SASI dominates over neutrino-driven convection (Kuroda et al. 2016; Andresen et al. 2017). The detection of these distinct GW features could help infer which one is more dominant in the supernova engine, neutrino-driven convection or the SASI (Andresen et al. 2017). In order to discuss the detectability of the signals, these studies have traditionally relied on the GW spectrum or spectrogram analysis using the information of the GW amplitude and the frequency only.

Hayama et al. (2016) were the first to point out the importance of detecting circular polarization of the GWs from CCSNe. They studied the GW polarization using results from Kuroda et al. (2014), where only a short duration ( $\sim 30$  ms) after bounce was followed in 3D general-relativistic (GR) models of a  $15M_{\odot}$  star, where the initial rotation rates were added to the non-rotating progenitor in a parametric manner. It was found that the clear signature of the GW polarization appears only for their most rapidly rotating model (assuming the initial angular velocity of  $\pi$  rad/s in the core). While novel, this finding may raise several questions. These include whether the GW polarization could or could not be generated from canonical (essentially, non-rotating) progenitors, how far the GW polarization, if generated, would be detectable in the four-detector era, and what we can learn about the supernova engine from the future detection of the GW polarization.

In this work, we aim to answer these questions by studying the GW circular polarization using results from 3D full GR core-collapse simulations following  $\sim 300$  ms after bounce (Kuroda et al. 2016). For the signal detection, we perform a coherent network analysis where the network of LIGO Hanford, LIGO Livingston (L), VIRGO (V), and KAGRA (K) is considered (Hayama et al. 2015). We find that the amplitude of the GW circular polarization becomes much bigger for our 3D-GR model that exhibits a strong SASI activity. We will show that the GW circular polarization, if detected, could provide a new probe to decipher the inner-working of the supernova engine.

## 2 NUMERICAL METHODS AND INITIAL MODELS

We analyse the GW predictions from 3D-GR supernova models in Kuroda et al. (2016) who followed the hydrodynamics from the onset of core-collapse of a  $15M_{\odot}$  star (Woosley & Weaver 1995), through core bounce, up to  $\sim 300$  ms after bounce. In the simulation, the BSSN formalism is employed to evolve the metric (Shibata & Nakamura 1995; Baumgarte & Shapiro 1999), and the GR neutrino transport is solved by an energy-integrated M1 scheme (Kuroda et al. 2012). The 3D computational domain is a cubic box with 15,000 km where the nested boxes with 8 refinement levels are embedded. Each box contains  $128^3$  cells and the minimum grid size near the origin is  $\Delta x = 458$  m.

We choose two representative models from Kuroda et al. (2016), one with the nuclear equation of state (EOS) of SFHx (Steiner et al. 2013) and another of TM1 by Hempel & Schaffner-Bielich (2010). In the following, we refer to the two models as SFHx and TM1, respectively. For SFHx and

TM1, the maximum gravitational mass ( $M_{\text{max}}$ ) and the radius ( $\bar{R}$ ) of a cold NS is  $M_{\text{max}} = 2.13$  and  $2.21 M_{\odot}$ , and  $\bar{R} = 12.0$  and  $14.5$  km, respectively, meaning that SFHx is softer than TM1. Note that SFHx is the best-fit model with the observational mass-radius relation of cold NSs (Steiner et al. 2010, 2013).

The 3D hydrodynamic evolution is rather similar between SFHx and TM1, which is characterized by the prompt convection phase shortly after bounce ( $T_{\text{pb}} \lesssim 20$  ms with  $T_{\text{pb}}$  the postbounce time), then the linear (or quiescent) phase ( $20 \lesssim T_{\text{pb}} \lesssim 140$  ms), which is followed by the non-linear phase when the SASI dominates over neutrino-driven convection in the postshock region ( $140 \lesssim T_{\text{pb}} \lesssim 300$  ms). The key difference is that the softer EOS (SFHx) makes the PNS radius and the shock radius at the shock-stall more compact than those of TM1. This leads to more stronger activity of the SASI for SFHx compared to TM1 (see Kuroda et al. (2016) for more details).

For extracting GWs, we employ a quadrupole formula proposed by Shibata & Sekiguchi (2003) for numerical relativity simulations. The transverse and the trace-free gravitational field is expressed as  $h_{ij} = (A_+(\theta, \phi)e_+ + A_{\times}(\theta, \phi)e_{\times})/D \equiv h_+e_+ + h_{\times}e_{\times}$ , where  $A_{+/\times}(\theta, \phi)$  represent amplitude of orthogonally polarized wave components with the emission angle  $(\theta, \phi)$ ,  $e_{+/\times}$  denote unit polarization tensors,  $D$  is the distance to the source. The circular polarization of GWs is described by the Stokes parameters (Seto & Taruya 2007), which is expressed by the combination of the right-handed ( $h_R \equiv (h_+ - ih_{\times})/\sqrt{2}$ ) and left-handed ( $h_L \equiv (h_+ + ih_{\times})/\sqrt{2}$ ) polarization modes (see Equation (1) of Hayama et al. (2016)). We focus on the Stokes  $V$  parameter, which directly characterizes the asymmetry between the right- and left-handed modes of the circular polarization.

Following Hayama et al. (2015), we perform a coherent network analysis of the four detectors (H, L, V, and K) using the RIDGE pipeline.<sup>1</sup> For simplicity, a Gaussian, stationary noise is assumed, which is produced by generating four independent realization of white noise and passing them through the finite impulse response filters having transfer functions which approximately match the design sensitivity curves of the detectors (taken from Sathyaprakash & Schutz (2009); Manzotti & Dietz (2012); Aso et al. (2013)). The injected signals correspond to a signal source located in the direction to the Galactic center, where arrival time to each detector is taken into account for the source localization with the angular resolution of  $d\Omega = 4 \times 4$  square degrees (see Hayama et al. (2015) for more detail).

## 3 RESULTS

Figure 1 summarizes the gravitational waveforms (top panels) and the spectrograms of the Stokes  $V$  parameter (bottom panels) for SFHx (left panels) and TM1 (right panels), respectively. After core bounce, one can see a ramp-up feature in the spectrogram of SFHx (the bottom left panel) before  $T_{\text{pb}} \sim 140$  ms, where the excess (colored by blue and red) increases from  $\sim 100$  to 500 Hz. This ramp-up

<sup>1</sup> See Logue et al. (2012); Gossan et al. (2016); Mukherjee et al. (2017) for representative studies using other pipelines.

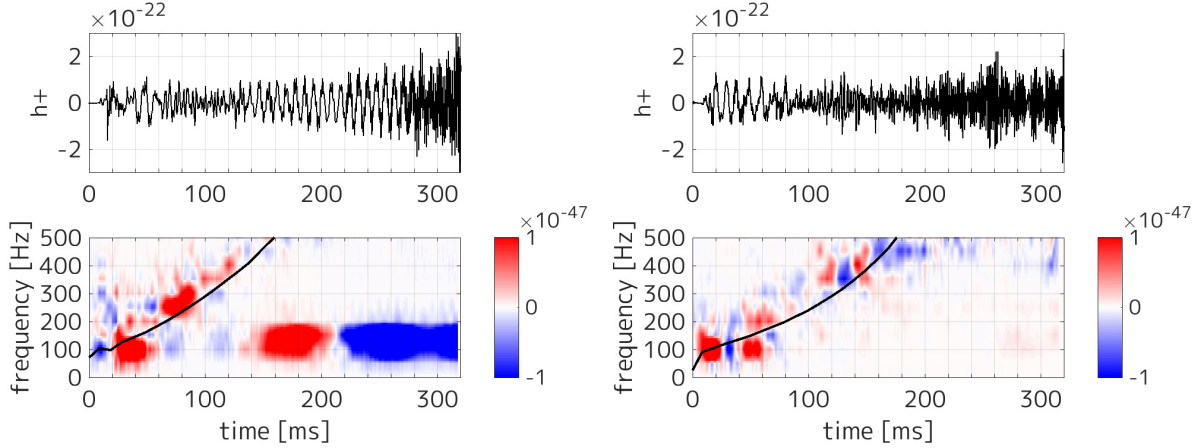
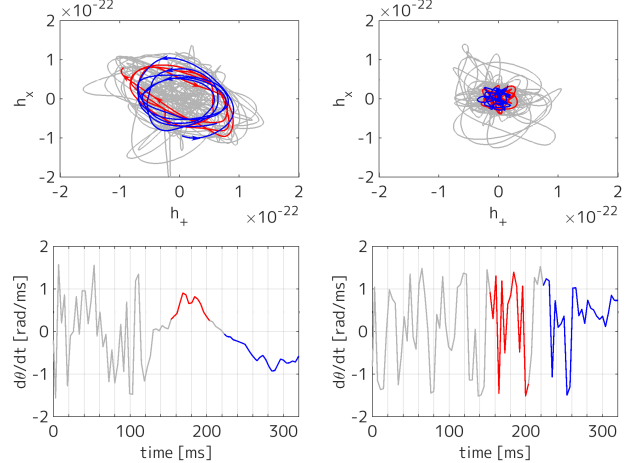


**Figure 1.** The top panels are the original gravitational waveforms ( $h_+$ ) and the bottom panels are the spectrograms for the Stokes  $V$  parameter of SFHx (left panels) and TM1 (right panels), respectively. The black line in the bottom panels corresponds to the peak GW frequency of the PNS  $g$ -mode oscillation (see also Figure 1 of Kuroda et al. (2016)). A source distance of  $D = 10$  kpc is assumed. The waveforms are extracted along the north pole  $(\theta, \phi) = (0, 0)$ . A series of short-time (20 ms) Fourier transformation are calculated to obtain the  $V$  parameter from the reconstructed waveforms at different times, which we refer to as the spectrogram.

component is clearly correlated with the peak frequency of the PNS surface oscillation (black line in the bottom panels, corresponding to  $F_{\text{peak}}$  defined in Müller et al. (2013)). Note that we focus on the frequency range below  $\sim 500$  Hz in the spectrogram, because the higher frequency domain is difficult to detect due to a shot-noise of the laser interferometers. The ramp-up feature is also seen for TM1 (the bottom right panel) for a longer period ( $T_{\text{pb}} \lesssim 180$  ms). The PNS surface oscillation, primarily driven by buoyancy (Murphy et al. 2009), occurs in a stochastic manner. Consequently, the sign of the circular polarization changes stochastically. In fact, the ramp-up signature of the  $V$  parameter ( $T_{\text{pb}} \lesssim 180$  ms in the bottom panels) is a mixture of right-handed (colored by red) and left-handed (colored by blue) modes, where the right-handed mode is by chance stronger for SFHx.

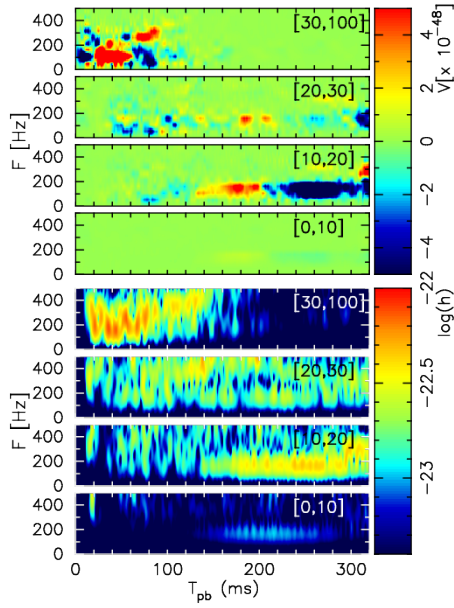
At  $140 \lesssim T_{\text{pb}} \lesssim 300$  ms, the waveform of SFHx shows a quasi-periodic modulation (the top left panel), which is not present in the waveform of TM1 (the top right panel). As previously identified, this signature is a result of the SASI-induced mass accretion flows striking the PNS core surface (e.g., Kuroda et al. (2016); Andresen et al. (2017)). In the SASI-dominant phase, the  $V$ -mode spectrogram for SFHx (the bottom left panel) shows a clear excess of the right-handed polarization first (colored by red,  $140 \lesssim T_{\text{pb}} \lesssim 200$  ms), which is followed by a clear excess of the left-handed polarization (colored by blue,  $220 \lesssim T_{\text{pb}} \lesssim 320$  ms). Between the two epochs, a quiescent phase with vanishing polarization amplitude (white in the panel) is observed between  $200 \lesssim T_{\text{pb}} \lesssim 220$  ms.

Figure 2 visualizes the time evolution of the GW circular polarization of SFHx (left panels) and TM1 (right panels). Note in each panel that the two SASI-dominant phases of SFHx are colored by red or blue, corresponding to the bottom left panel of Figure 1 at  $T_{\text{pb}} \gtrsim 140$  ms. One can see a clearer polarization signature for SFHx (the top left panel) characterized by the bigger GW amplitude with the right-handed (red line) and left-handed mode (blue line) than those for TM1 (the top right panel). Before  $T_{\text{pb}} \sim 140$



**Figure 2.** The top panels show the trajectory of the GW polarization on the  $h_+ - h_\times$  plane of SFHx (left panel) and TM1 (right panel). Making a correspondence to the bottom left panel of Figure 1, the two characteristic epoch with the right-handed ( $140 \lesssim T_{\text{pb}} \lesssim 200$  ms) and left-handed ( $220 \lesssim T_{\text{pb}} \lesssim 320$  ms) polarization are highlighted with the red and blue color. The gray line denotes the whole trajectory during the simulation time. Similar to the top panels, but the bottom panels depict the time derivative of the polarization angle ( $d\theta/dt$ ). The polarization angle  $\theta$  is measured from the axis of  $h_\times$  as  $\theta \equiv \arctan(h_+/h_\times)$  spanning  $0 \leq \theta \leq \pi$  and  $0 \geq \theta \geq -\pi$ , respectively. Note that the signals are low-pass filtered with a cutoff frequency of 400Hz to focus on the low-frequency behaviors.

ms, the bottom left panel shows that the time derivative of the polarization angle ( $d\theta/dt$ ) changes randomly with time, taking both positive and negative values of  $d\theta/dt$ . But, after  $T_{\text{pb}} \sim 140$  ms when the SASI activity begins to be vigorous (e.g., Kuroda et al. (2016)), the right-handed GW polarization (e.g., the red line in the bottom left panel) is shown to transit to the left-handed polarization (the blue line) until  $T_{\text{pb}} \sim 320$  ms, after which neutrino-driven convection dom-



**Figure 3.** Contributions from four spherical shells with intervals of  $[0, 10]$ ,  $[10, 20]$ ,  $[20, 30]$ , and  $[30, 100]$  km to the GW circular polarization (top panels) and the GW amplitude (bottom panels) of SFHx, respectively. The source is assumed at a distance of 10 kpc.

inates over the SASI. The bottom right panel shows that the value of  $d\theta/dt$  of TM1 changes more stochastically during the simulation time, making the net circular polarization very small (e.g., the top right panel of Figure 2 and bottom right panel of Figure 1).

From the spectrogram of SFHx (the bottom left panel of Figure 1), one can clearly see that the typical frequency of the strong circular polarization is in the range of  $100 \sim 200$  Hz, which is in the best sensitivity range of the LIGO-class detectors. We thus focus on the GW signatures of SFHx in the following.

To clarify the origin of the circular polarization in the postbounce core, we plot in Figure 3 contributions from representative four spherical shells to the circular polarization (the top panels) and the GW amplitude (the bottom panels) of SFHx, respectively. From the PNS core surface region (see the panels labeled with  $[10, 20]$  km), the excess in the circular polarization (see the horizontal stripe colored in red or blue in the top panel) is correlated with the GW emission at the low-frequency domain of  $100 - 200$  Hz (colored by yellow or red in the bottom panel). This low-frequency component is identified to originate from the SASI-induced flows penetrating into the PNS core (Kuroda et al. 2016; Andresen et al. 2017). From between the PNS and the shock (see panels labeled with  $\sim [30, 100]$  km), one can also see that the ramp-up  $g$ -mode of the PNS oscillation (e.g., the red and yellow region in the bottom panel at  $0 \lesssim T_{\text{pb}} \lesssim 140$  ms) has a significant overlap with the excess in the  $V$  parameter (the top panel). These findings illuminate the importance of detecting the GW polarization because the pre-explosion hydrodynamical features such as the SASI activity and the PNS oscillation are clearly imprinted in the spectrogram.

Following Hayama et al. (2015), we quantify the detectability of the GW signatures by performing Monte Carlo

simulations, where the network of H, L, V, and K is considered. The  $V$ -mode is calculated by the reconstructed  $h_+$  and  $h_\times$ . The top panels of Figure 4 shows a *time-frequency* signal-to-noise ratio ( $\text{SNR}_{\text{TF}}$ ) of the reconstructed GW waveform, which is defined as  $\text{SNR}_{\text{TF}} \equiv I(s+n)/\sqrt{\langle I(n) - \langle I(n) \rangle \rangle^2}$  with  $I(x)$  the Stokes  $I$  parameter (e.g., Eq.(1) in Hayama et al. (2016)),  $s$  the signal, and  $n$  the Gaussian noise,  $\langle x \rangle$  denotes the time average of  $x$ , respectively. By setting the (optimal) detection threshold as 10, the top panels of Figure 4 show that the detection horizon even using the four detectors can only reach to a several kpc (e.g., the top left panel for a source at 2kpc). By replacing  $I$  of  $\text{SNR}_{\text{TF}}$  with  $|V|$ , we estimate the SNR of the circular polarization ( $\text{SNR}_{\text{CP}}$ ). From the bottom panels of Figure 4, one can see that the SNR of the circular polarization is significantly higher than  $\text{SNR}_{\text{TF}}$ . For a source at 10 kpc (the bottom right panel),  $\text{SNR}_{\text{CP}}$  exceeds the fiducial threshold for the low-frequency component, which cannot be detectable solely by looking for the excess in the GW spectrogram (the top right panel). The significant enhancement of  $\text{SNR}_{\text{CP}}$  comparing with  $\text{SNR}_{\text{TF}}$  is because the Gaussian noise (by nature) has little component of the circular polarization. From the bottom left panel, one can see that the circular polarization from the ramp-up component of the PNS oscillation is high ( $\text{SNR}_{\text{CP}} \sim 200$ ), which may allow detection for a nearby source such as at 2 kpc (the bottom left panel). These results demonstrate that the GW circular polarization could not only extend the detection horizon of the signal farther, but also provide a new probe to decipher the inner-working of the supernova engine such as the PNS oscillation and the SASI.

## 4 DISCUSSIONS

In this work, we considered only the idealized Gaussian noise. Effects of real non-Gaussian and nonstationary noise need to be considered (Powell et al. 2016, 2017). This is one of the most important tasks that we have to investigate as a sequel of this work. It is recently pointed out that there is a correlation between the SASI-induced modulation in the GW and neutrino signals (Kuroda et al. 2017; Tamborra et al. 2013). The correlation between the neutrino signal and the GW circular polarization would deserve further investigation. Using a single progenitor model and the particular EOS (SFHx), we found that the strong SASI activity and the PNS oscillation are imprinted in both the waveform and the circular polarization. In order to clarify how general this trend would be, a systematic 3D CCSN simulation changing the progenitor models and EOSs is needed to be done. This is a grand computational challenge, which we shall leave as future work. Consideration of the circular polarization into the GW search pipeline is also urgent, which could significantly enhance the chance of detecting a CCSN GW in the future.

## ACKNOWLEDGEMENTS

We are thankful to S. Yamada, H. Kawahara and N. Kanda for stimulating discussions. Numerical computations were carried out in part on XC30 at the CfCA of NAOJ. This



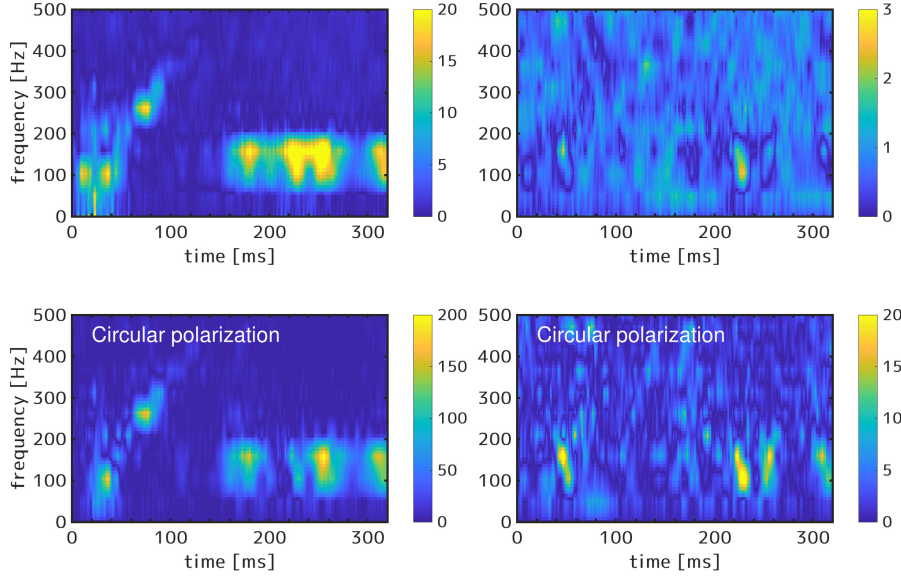


**Figure 4.** Time-frequency signal-to-noise ratio of the reconstructed waveform ( $\text{SNR}_{\text{TF}}$ , top panels) and the circular polarization ( $\text{SNR}_{\text{CP}}$ , bottom panels) for a source at 2 kpc (left panels) and at 10 kpc (right panels), respectively (see text). Note that the excess changes slightly with the distance because the noise impacts non-linearly the phase between  $h_+$  and  $h_\times$ .

study was supported by JSPS KAKENHI Grant Number (JP15H00789, JP15H01039, JP17H05206, JP17K14306, JP17H01130, JP17H06364), and by the Central Research Institute of Fukuoka University (Nos.171042, 177103), and JICFuS as a priority issue to be tackled by using the Post ‘K’ Computer.

## REFERENCES

- Abbott B. P., et al., 2016, *Living Reviews in Relativity*, **19**, 1
- Abbott B. P., et al., 2017, *Physical Review Letters*, **119**, 141101
- Akutsu T., et al., 2017, preprint, ([arXiv:1712.00148](#))
- Andresen H., Müller B., Müller E., Janka H.-T., 2017, *MNRAS*, **468**, 2032
- Aso Y., Michimura Y., Somiya K., Ando M., Miyakawa O., Sekiguchi T., Tatsumi D., Yamamoto H., 2013, *Phys. Rev. D*, **88**, 043007
- Baumgarte T. W., Shapiro S. L., 1999, *Phys. Rev. D*, **59**, 024007
- Cerdá-Durán P., DeBrye N., Aloy M. A., Font J. A., Obergaulinger M., 2013, *ApJ*, **779**, L18
- Gossan S. E., Sutton P., Stuver A., Zanolini M., Gill K., Ott C. D., 2016, *Phys. Rev. D*, **93**, 042002
- Hayama K., Kuroda T., Kotake K., Takiwaki T., 2015, *Phys. Rev. D*, **92**, 122001
- Hayama K., Kuroda T., Nakamura K., Yamada S., 2016, *Physical Review Letters*, **116**, 151102
- Heger A., Woosley S. E., Spruit H. C., 2005, *ApJ*, **626**, 350
- Hempel M., Schaffner-Bielich J., 2010, *Nuclear Physics A*, **837**, 210
- Janka H.-T., 2017, preprint, ([arXiv:1702.08825](#))
- Kotake K., 2013, *Comptes Rendus Physique*, **14**, 318
- Kotake K., Iwakami W., Ohnishi N., Yamada S., 2009, *ApJ*, **697**, L133
- Kuroda T., Kotake K., Takiwaki T., 2012, *ApJ*, **755**, 11
- Kuroda T., Takiwaki T., Kotake K., 2014, *Phys. Rev. D*, **89**, 044011
- Kuroda T., Kotake K., Takiwaki T., 2016, *ApJ*, **829**, L14
- Kuroda T., Kotake K., Hayama K., Takiwaki T., 2017, *ApJ*, **851**, 62
- Logue J., Ott C. D., Heng I. S., Kalmus P., Scargill J. H. C., 2012, *Phys. Rev. D*, **86**, 044023
- Manzotti A., Dietz A., 2012, preprint, ([arXiv:1202.4031](#))
- Morozova V., Radice D., Burrows A., Vartanyan D., 2018, preprint, ([arXiv:1801.01914](#))
- Mukherjee S., Salazar L., Mittelstaedt J., Valdez O., 2017, *Phys. Rev. D*, **96**, 104033
- Müller E., Janka H.-T., 1997, *A&A*, **317**, 140
- Müller E., Rampp M., Buras R., Janka H.-T., Shoemaker D. H., 2004, *ApJ*, **603**, 221
- Müller B., Janka H.-T., Marek A., 2013, *ApJ*, **766**, 43
- Murphy J. W., Ott C. D., Burrows A., 2009, *ApJ*, **707**, 1173
- Ott C. D., 2009, *Classical and Quantum Gravity*, **26**, 063001
- Ott C. D., et al., 2013, *ApJ*, **768**, 115
- Powell J., Gossan S. E., Logue J., Heng I. S., 2016, *Phys. Rev. D*, **94**, 123012
- Powell J., Szczepanczyk M., Heng I. S., 2017, preprint, ([arXiv:1709.00955](#))
- Sathyaparakash B. S., Schutz B. F., 2009, *Living Reviews in Relativity*, **12**, 2
- Seto N., Taruya A., 2007, *Physical Review Letters*, **99**, 121101
- Shibata M., Nakamura T., 1995, *Phys. Rev. D*, **52**, 5428
- Shibata M., Sekiguchi Y.-I., 2003, *Phys. Rev. D*, **68**, 104020
- Steiner A. W., Lattimer J. M., Brown E. F., 2010, *ApJ*, **722**, 33
- Steiner A. W., Hempel M., Fischer T., 2013, *ApJ*, **774**, 17
- Summa A., Janka H.-T., Melson T., Marek A., 2017, preprint, ([arXiv:1708.04154](#))
- Takiwaki T., Kotake K., Suwa Y., 2016, *MNRAS*, **461**, L112
- Tamborra I., Hanke F., Müller B., Janka H.-T., Raffelt G., 2013, *Physical Review Letters*, **111**, 121104
- Woosley S. E., Weaver T. A., 1995, *ApJS*, **101**, 181
- Yakunin K. N., et al., 2015, *Phys. Rev. D*, **92**, 084040
- Yakunin K. N., et al., 2017, preprint, ([arXiv:1701.07325](#))